Antarctic iceberg melt rate variability and sensitivity to ocean thermal forcing

Ellyn M. Enderlin[1,2] ![ID], Carlos Moffat[3] ![ID], Emily Miller[2], Adam Dickson[1], Caitlin Oliver[1], Mariama C. Dryák-Vallies[2,4] and Rainey Aberle[1] ![ID]

[1]Boise State University, Boise, Idaho, USA; [2]University of Maine, Orono, Maine, USA; [3]University of Delaware, Newark, Delaware, USA and [4]University of Colorado Boulder, Boulder, Colorado, USA

Abstract

Changes in iceberg calving fluxes and oceanographic conditions around Antarctica have likely influenced the spatial and temporal distribution of iceberg fresh water fluxes to the surrounding ocean basins. However, Antarctic iceberg melt rate estimates have been limited to very large icebergs in the open ocean. Here we use a remote-sensing approach to estimate iceberg melt rates from 2011 to 2022 for 15 study sites around Antarctica. Melt rates generally increase with iceberg draft and follow large-scale variations in ocean temperature: maximum melt rates for the western peninsula, western ice sheet, eastern ice sheet and eastern peninsula are ~50, ~40, ~5 and ~5 m a^{-1}, respectively. Iceberg melt sensitivity to thermal forcing varies widely, with a best-estimate increase in melting of ~24 m a^{-1}°C^{-1} and range from near-zero to ~100 m a^{-1}°C^{-1}. Variations in water shear likely contribute to the apparent spread in thermal forcing sensitivity across sites. Although the sensitivity of iceberg melt rates to water shear prevents the use of melt rates as a proxy to infer coastal water mass temperature variability, additional coastal iceberg melt observations will likely improve models of Southern Ocean fresh water fluxes and have potential for subglacial discharge plume mapping.

Introduction

Oceanic warming has been implicated as the primary driver of dynamic mass loss around nearly all of Antarctica, influencing the stability of floating ice tongues and ice shelves fringing the West and East Antarctic Ice Sheets (WAIS and EAIS) and the East Antarctic Peninsula (EAP) (Glasser and Scambos, 2008; McGrath and others, 2012; Pritchard and others, 2012; DePoorter and others, 2013; Khazendar and others, 2013; Greenbaum and others, 2015; Jeong and others, 2016; Holland and others, 2020) as well as the grounded marine-terminating glaciers along the West Antarctic Peninsula (WAP) (Cook and others, 2016). Approximately half of the fresh water flux from continental Antarctica is in the form of icebergs (Rignot and others, 2013) and dynamic mass loss is often triggered by or results in an increase in iceberg production (e.g. Larsen B ice shelf 'disintegration' and subsequent accelerated dynamic mass loss from tributary glaciers (Scambos and others, 2004, 2014; Shuman and others, 2011)). As icebergs drift away from their sources, their physical fragmentation and melt result in the redistribution of their fresh water across the Southern Ocean. Coupled iceberg–ocean models have demonstrated that iceberg melt has a significant impact on the physical properties of water masses and, in turn, sea-ice extent and Antarctic Bottom Water formation (Jongma and others, 2009; Merino and others, 2016; England and others, 2020). Meltwater from drifting icebergs also strongly influences the chemical and biological properties of ocean water (Smith and others, 2007, 2013; Schwarz and Schodlok, 2009; Wu and Hou, 2017; Hopwood and others, 2019).

Despite the importance of iceberg meltwater on the physical, chemical and biological properties of ocean masses around Antarctica and the potential changes in meltwater fluxes over the last several decades, Antarctic iceberg melt rates are poorly constrained. Satellite observations of large iceberg decay during their months- to years-long residence in the Antarctic Coastal Current and open ocean suggest that there is near-zero melt during the austral winter and that the melt rate peaks at ~0.25–1.5 m d^{-1} during the austral summer (Tournadre and others, 2012; Bouhier and others, 2018). Coupled iceberg–ocean models are capable of reproducing the open ocean melt rates and trajectories when the iceberg melt rate is prescribed as a function of the difference between the temperature of the water and its freezing point ($T_w - T_{fp}$), often referred to as thermal forcing, and the shear velocity of the water with respect to the iceberg (Jongma and others, 2009; Merino and others, 2016; England and others, 2020). Specifically, these models often rely on the Weeks and Campbell (1973) melt equation, wherein the melt rate ($\dot{m}$) is parameterized as

$$\dot{m} = 0.037 \left(\frac{\rho_w}{\rho_i} v^{\frac{-7}{15}} \kappa^{\frac{2}{3}} \frac{c_w}{\Lambda} \right) \frac{U_{rel}^{\frac{4}{5}}(T_w - T_{fp})}{L^{\frac{1}{5}}} \qquad (1)$$

where ρ_w and ρ_i are the densities of water and ice, v is the diffusivity of momentum, κ is the diffusivity of temperature, c_w is the specific heat of water, Λ is the latent heat of melting, U_{rel} is

the relative velocity of the iceberg with respect to the water, $(T_w - T_{fp})$ is the thermal forcing estimated as the difference between the water temperature T_w and the freezing point T_{fp}, and L is the length of the long axis of the iceberg. However, given the coarse spatial resolution of the coupled ice–ocean models (~0.2–3° or ~20–350 km), they are unlikely to accurately estimate iceberg melt rates or meltwater fluxes in coastal regions, motivating the need for remotely sensed iceberg melt estimates.

Here we expand on the limited estimates of Antarctic iceberg melt rates using a remotely sensed surface elevation-differencing approach previously applied to icebergs calved from the Greenland Ice Sheet (Enderlin and others, 2016, 2018). We describe spatial and temporal variations in iceberg melt rates for 15 sites distributed around Antarctica using satellite imagery from 2011 to 2022 (Fig. 1; Table 1). Additionally, we compare these melt rates to in situ ocean temperature data to assess relationships between variations in iceberg melt rates and ocean thermal forcing. We conclude with a discussion of the apparent sensitivity of iceberg melting to variations in ocean conditions, with recommendations for future analyses of iceberg melting as

a tool to better understand changing ice–ocean interactions in the Antarctic and beyond.

Data and methods

Iceberg melt rates

Iceberg melt rates were estimated using a remotely sensed elevation-differencing approach for 15 study sites around Antarctica (Fig. 1; Table 1). Spatial and temporal coverage of iceberg melt rate estimates were limited by the availability of the high-resolution (~0.5 m) commercial WorldView imagery used to create time series of iceberg surface elevations. Although WorldView imagery is available from 2011 to 2022, the iceberg melt time series is seasonally limited by solar illumination, with further spatio-temporal limitations due to the irregular timing of iceberg movements, relatively small footprint of the satellite images (~290 km²), and sporadic satellite image acquisitions. Since iceberg identification and delineation is performed manually, iceberg melt rate estimation is a labor-intensive process. To optimize the number of icebergs in our dataset, we focused on WorldView images
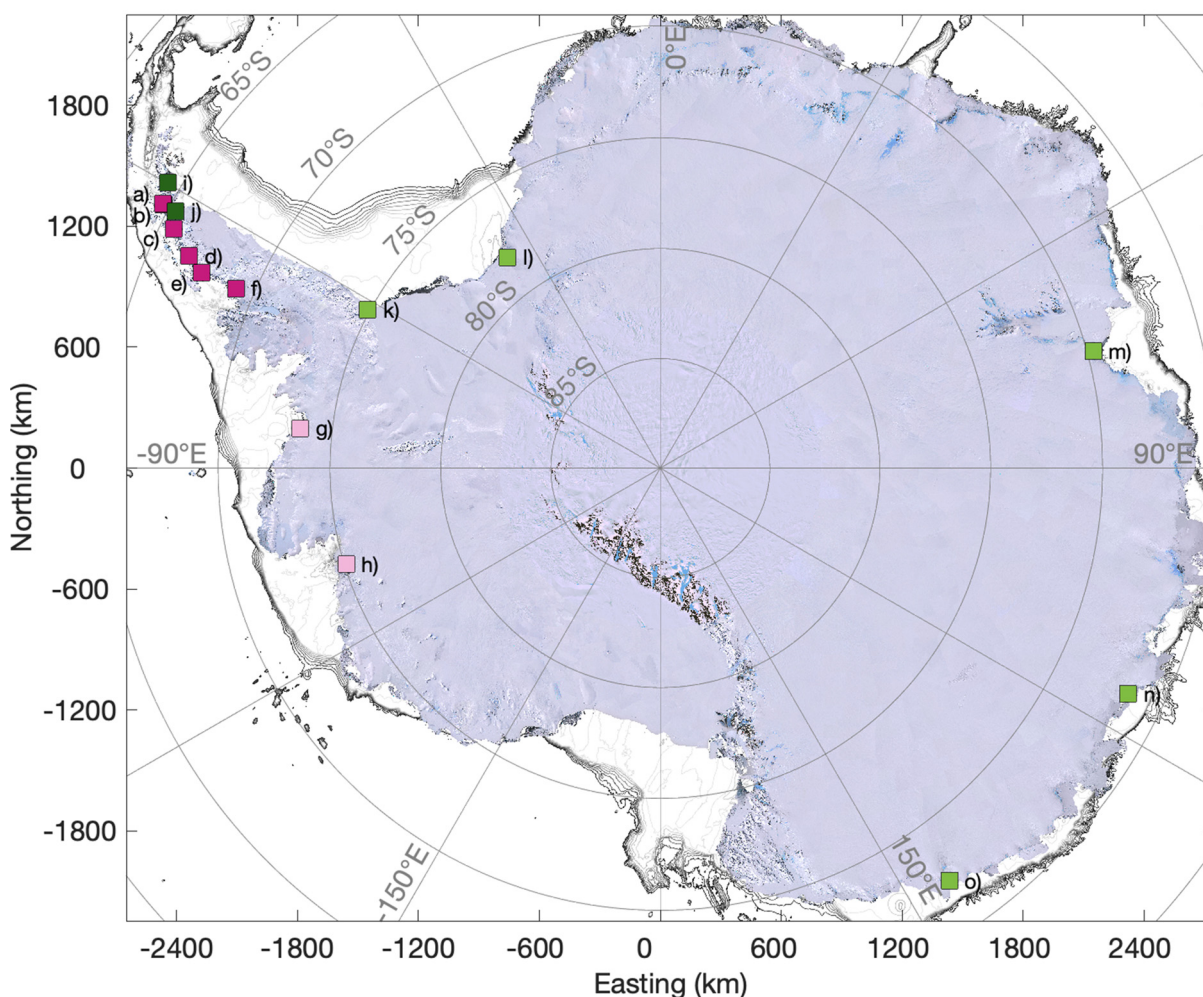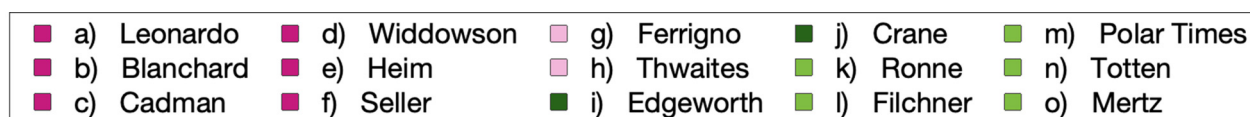

Figure 1. Map of study sites. The colors distinguish geographic regions: dark pink for the West Antarctic Peninsula (WAP), light pink for the West Antarctica Ice Sheet (WAIS), light green for the East Antarctic Ice Sheet (EAIS) and dark green for the East Antarctic Peninsula (EAP). Bathymetric contours at 250 m depth increments down to 2500 m-depth are shown as light gray lines, with darker lines indicating greater depths. The continental shelf break is visible as closely spaced dark gray lines. Site names were obtained from the Scientific Committee on Antarctic Research Composite Gazetteer of Antarctica. The background image is the Landsat Image Mosaic for Antarctica (Bindschadler and others, 2008).

Table 1. Summary of iceberg melt observations

Site name	Observation dates	Iceberg count	Easting (m) Minimum	Maximum	Northing (m) Minimum	Maximum	Draft (m b.s.l.) Median	Minimum	Maximum	Melt rate (m a^{-1}) Median	Minimum	Maximum
Edgeworth	2013/09/01-2014/10/26	15	−2448050	−2443900	1413150	1416800	176	95	216	1.3	0.3	19.9
	2014/10/26-2015/08/31	15	−2445950	−2434450	1413100	1418250	142	87	180	1.3	0.1	3.3
	2015/08/31-2016/09/04	17	−2446700	−2437000	1412250	1418200	142	82	165	1.1	0.1	10.5
	2017/04/16-2018/04/28	12	−2446950	−2442550	1413550	1417300	40	22	82	0.7	0.2	1.3
	2018/04/28-2019/01/24	14	−2447100	−2443550	1413650	1417550	74	28	145	1.4	0	2.1
	2019/10/13-2020/09/28	16	−2446000	−2437801	1414300	1418449	98	59	179	0.6	0.2	3.7
Crane	2013/03/03-2014/04/15	13	−2408250	−2402050	1267300	1278050	91	39	187	0.8	0	2.9
	2014/04/15-2015/09/15	18	−2406950	−2400550	1274850	1279850	121	40	194	0.7	0.2	2.4
	2015/09/15-2016/01/18	12	−2406250	−2401300	1274500	1280150	122	83	174	1.7	0.6	4.3
	2016/01/18-2017/01/08	11	−2406950	−2400850	1270600	1277750	136	86	191	0.4	0.2	1.4
	2017/01/08-2019/11/20	13	−2405000	−2400650	1271050	1282300	187	102	260	0.6	0.2	5.1
Ronne	2014/11/19-2016/10/04	12	−1453750	−1446000	777235	786245	117	53	134	2.2	0.9	2.8
	2016/10/04-2018/01/05	12	−1454450	−1447950	778890	790335	100	71	118	3	0.9	7.3
	2018/01/05-2020/01/11	5	−1459150	−1455300	790910	795640	125	124	132	2.5	2.1	3.2
	2018/01/05-2020/02/06	2	−1453450	−1450900	781465	784315	148	148	149	1.7	1.6	1.9
	2020/11/06-2022/02/06	9	−1454431	−1444727	775743	781290	35	26	76	2	0.2	4.6
Filchner	2013/12/10-2015/09/14	12	−759365	−755145	1043750	1046800	143	88	192	2	0	3.8
	2015/09/14-2017/11/04	13	−760180	−754550	1042850	1047800	118	71	189	1.7	0.3	2.5
	2017/11/04-2020/01/10	8	−760910	−755900	1044900	1049800	140	88	185	1.7	0.9	2.9
Polar Times	2015/04/03-2017/03/26	12	2146200	2150950	575915	585760	130	101	234	1.6	0.5	2.3
	2017/01/01-2018/05/04	15	2141400	2151000	574775	581035	177	99	231	2	0.6	3.6
	2018/03/06-2019/09/27	15	2147500	2152750	577810	581950	160	123	218	2.2	1	3.6
	2020/10/27-2021/11/10	19	2143642	2157125	575485	589171	140	66	222	1.7	0.1	6.7
Totten	2011/11/09-2015/03/31	14	2322700	2326800	−1123200	−1120400	98	29	147	2.5	1.5	3.6
	2016/09/29-2018/03/17	16	2319050	2327750	−1129700	−1117400	131	64	370	2.9	1.7	7.3
	2018/03/17-2020/01/29	16	2318300	2328450	−1127650	−1114850	188	83	284	3.2	2.7	4.9
Mertz (West)	2016/03/23-2018/03/25	12	1442150	1447200	−2046100	−2040950	185	92	216	2.6	0.3	4.9
	2018/03/25-2020/01/10	9	1442300	1445800	−2047000	−2041200	227	159	311	2.7	1.9	3.6
	2020/01/10-2022/01/12	7	1443096	1446238	−2046430	−2044068	122	88	158	1.7	0.9	3.2
Mertz (East)	2021/03/01-2022/01/09	6	1392437	1398870	−2079920	−2075860	364	310	467	14.8	4	35
Thwaites (West)	2016/02/23-2017/12/22	33	−1548750	−1533100	−485755	−470910	399	183	627	17.1	7.6	29.6
	2017/10/14-2018/01/16	11	−1587850	−1569900	−487470	−480940	312	174	352	6.1	0.7	8.6
	2019/10/12-2020/01/24	54	−1582800	−1533650	−494065	−468460	363	108	744	15.3	0.8	42.3
	2020/01/24-2020/10/08	36	−1564332	−1549301	−488220	−476317	195	97	438	8.2	3.9	19.1
Thwaites (East)	2014/10/28-2016/11/02	16	−1580750	−1572750	−467075	−456810	257	144	299	2.2	1	3.6
	2016/11/02-2018/01/11	12	−1584000	−1575550	−462685	−453720	217	143	264	1.2	0.5	3.8
	2018/01/24-2019/10/23	5	−1559150	−1557250	−462220	−459740	245	185	287	5.1	2.2	7.6
Ferrigno	2017/01/17-2017/12/17	11	−1789250	−1783500	196430	206155	129	79	200	5.3	1.4	11.4
	2018/01/24-2019/02/20	8	−1788300	−1784350	196355	201385	185	151	224	5.1	1.6	9.5
	2019/02/20-2020/01/26	6	−1787800	−1784450	193880	198650	152	131	198	8.8	2.8	14.9
Seller	2014/11/25-2016/01/19	15	−2116750	−2106050	888690	898215	97	74	160	14.5	8.6	23
	2016/01/19-2017/09/16	16	−2113150	−2104650	893695	897955	63	47	102	5.8	0.7	15
	2019/01/26-2019/03/01	11	−2105900	−2101750	885390	891260	149	78	247	18.9	9.1	62.6
	2019/09/15-2019/11/04	24	−2110404	−2099492	881994	896282	109	56	178	18.6	0.6	46.6
Heim	2015/09/19-2016/02/13	9	−2276800	−2275600	964205	965260	27	12	55	1.5	0.4	12.9
	2020/09/27-2021/01/10	21	−2279817	−2277013	965551	971225	37	21	91	3.6	0.4	10.5
Widdowson	2016/08/21-2017/02/18	16	−2341700	−2335050	1050950	1054450	56	33	94	16.5	7.1	33.9
	2018/12/09-2019/03/01	14	−2339900	−2334450	1051300	1053800	60	26	82	18.1	6.9	39.8
Cadman	2016/11/11-2017/01/19	13	−2417200	−2414350	1185450	1189400	46	18	92	12.1	1.3	29.9
	2018/11/10-2019/01/17	11	−2415850	−2414400	1189550	1190950	43	26	151	15.7	0.9	38.8
	2019/10/05-2019/12/16	8	−2420850	−2414750	1185000	1190800	76	51	176	27.9	21.2	47.2
	2020/10/14-2021/01/23	10	−2418986	−2410946	1183932	1188955	51	39	77	16.3	6.9	23.4
Blanchard	2016/08/26-2016/10/19	4	−2466500	−2465100	1307000	1308500	41	36	46	5.3	3.1	10.4
Leonardo	2016/08/26-2016/10/19	9	−2468100	−2466350	1310300	1313150	35	30	78	10.9	3.7	21.6

For each study site (column 1), the image acquisition dates (column 2; YYYY/MM/DD), number of iceberg observations (column 3), bounding box polar stereographic coordinates for all icebergs (columns 4–5) and metrics characterizing the drafts and melt rates of the icebergs (columns 6 and 7, respectively) are listed.

that partially overlapped terrestrial ice margins, where icebergs are most abundant and the presence of sea ice and/or ice mélange retards iceberg movement for at least a portion of the year. The five sites along the WAP have the sparsest temporal coverage due to persistent cloud cover and the rapid seasonal break-up of sea ice and subsequent evacuation of icebergs from the fjords. Elsewhere in Antarctica, icebergs remain in close proximity to their sources for longer time periods, enabling the construction of interannual melt rate time series for two sites along the WAIS and five sites along the EAIS, as well as two sites from the EAP. The Antarctic Peninsula study sites are the same as in Dryak and Enderlin (2020), updated to include data from 2019 to 2022.

The elevation-differencing approach is described in detail in Enderlin and Hamilton (2014), with modifications to estimate bulk iceberg density using the firn density model for Antarctica (Ligtenberg and others, 2011) described in Dryak and Enderlin (2020). Briefly, icebergs were manually identified and delineated in repeat high-resolution WorldView stereo images and their associated digital elevation models (DEMs) generated using the Ames Stereo Pipeline (Shean and others, 2016). Only along-track stereo images from the same acquisition date were used to generate DEMs, with the repeat interval dictated by image pair availability and iceberg drift rates as described above. Up to ∼20 icebergs broadly distributed across the images were delineated for each date pair, with preference given to larger icebergs. Surface

elevations integrated over the manually delineated iceberg area were converted to an iceberg volume estimate using modeled firn air content and pore close-off depths from the Ligtenberg and others (2011) firn density estimates, accounting for saturation of the firn with ocean water in all non-tabular icebergs. The submarine meltwater flux was then estimated as the change in iceberg volume over time, accounting for volume change from surface meltwater runoff and creep thinning. Finally, meltwater flux estimates were normalized by the estimated submerged surface area to yield the area-averaged melt rate perpendicular to the submerged ice face.

Uncertainties in meltwater flux and melt rate were estimated using standard error propagation techniques, as described in Enderlin and Hamilton (2014). Uncertainty in iceberg bulk density is the largest contributor to meltwater flux uncertainty. Density uncertainty was estimated from the 95% confidence interval for the exponential curve that was fit to the density profiles from the firn model. As such, density uncertainty varies with the thickness of the firn column relative to the full iceberg thickness. Although density uncertainty also contributes to uncertainty in iceberg draft and submerged area, temporal variations in draft and submerged area estimates exceed error-propagated uncertainties and we used the range in draft and submerged area relative to their time-averaged values to conservatively estimate uncertainties. Melt rate uncertainties account for both uncertainties in meltwater flux as well as temporal variations in submerged area.

Ocean data

Ocean observations are relatively sparse in both space and time, particularly over the continental shelf (Schmidtko and others, 2014; Jenkins and others, 2016; Moffat and Meredith, 2018; Sallée, 2018). Existing datasets include conductivity, temperature and depth (CTD) data collected from research cruises, but data near ice margins are scarce. Autonomous pinniped observations are restricted based on both logistical challenges as well as the feeding habits of the animals (Treasure and others, 2017). Time series from moored arrays remain sparse in time and space, and because of the dangers of sea ice and icebergs near the surface, mooring-derived ocean observations typically do not extend to the surface (e.g. Heywood and others, 2012). Here, we combined ocean data from multiple observational platforms and data-assimilating numerical model outputs in an effort to minimize the impact of ocean data availability on our analysis.

Ocean temperature profiles were compiled from all World Ocean Database CTD datasets and autonomous pinniped bathythermographs (APBs) located within ∼100 km from the iceberg sites (Figs 2, S1; Table 2). Additional in situ ocean temperature data were obtained from a compilation of historical hydrographic data and ARGO floats within the same search radius (ARGO, 2000). The search radius was selected to maximize the number of sites with ocean observations while minimizing the number of observations acquired beyond the continental shelf. For each study site, all available ocean temperature and salinity profiles were linearly interpolated to a standard depth profile extending from the surface to 800 m-depth using a median depth increment from all observed profiles. When multiple profiles were collected for the same observation date, the standardized profiles were time-averaged. Hereafter, we refer to all the profiles interpolated to the standard depth profile as standardized, regardless of whether they are the average of multiple profiles or are the stand-alone profile for each date.

There are ocean observations for 10 of 15 locations with remotely sensed iceberg melt estimates (Figs 2, S1; Table 2): Leonardo, Blanchard, Cadman, Widdowson and Heim glaciers along the WAP; Thwaites Glacier along the WAIS; Mertz, Totten and Filchner ice shelves along the EAIS; and Edgeworth

Glacier along the EAP. Ship-based CTD data represent the majority of the ocean observation dataset, with CTD profiles for all nine sites between 2012 and 2022. There are also APB data for Thwaites Glacier and the Filchner Ice Shelf and ARGO data for the Totten Ice Shelf within the 2011–2022 study period. However, the temporal coverage of ocean profiles varies between study sites, with most ocean profile acquisitions outside of the iceberg melt rate observation periods (Fig. 2).

The standardized ocean profiles were used to estimate the temperature and salinity of the water masses near the icebergs following two different approaches depending on the temporal resolution of the iceberg melt observations. For iceberg melt estimates spanning one or more years (EAP, EAIS and most WAIS), we assume that interannual variations in ocean properties exceed seasonality and use ocean profiles within 1–2 years of the central iceberg observation date (Fig. 2, black circles) to create time-averaged ocean temperature and salinity profiles. For seasonal iceberg melt estimates, which are primarily along the WAP, we assumed that seasonality in ocean properties exceeds interannual variability (Moffat and Meredith, 2018), and used ocean profiles from the same season to create time-averaged ocean temperature and salinity profiles. The time-averaged temperature and salinity profiles for each iceberg were then used to estimate iceberg thermal forcing as the difference between the ocean temperature and the freezing temperature of the water. Given the sparse record of in situ ocean observations, we also explored the use ocean data from the 1/6-degree Southern Ocean State Estimate for 2013–2019 (Mazloff and others, 2010) as a tool to estimate thermal forcing, as described in the Supplementary material.

Results

Iceberg melt rates

Iceberg meltwater fluxes and melt rates vary with geometry and geography (Fig. 3; Table 1). Using a more limited dataset for the Antarctic Peninsula, Dryak and Enderlin (2020) observed that iceberg meltwater fluxes and melt rates generally increase with submerged area and keel depth (i.e. draft), respectively (Fig. 3). However, the relationship between melt rate and draft varies across the geographic regions. Icebergs calved from the Antarctic Peninsula (both WAP and EAP) rarely exceed 1 km^2 in submerged area and 250 m in keel depth (Fig. 3, dark pink and green, respectively). However, meltwater fluxes and melt rates for the WAP are approximately an order of magnitude greater than for the EAP study sites. Excluding outliers for Edgeworth Glacier, a former Larsen A ice shelf tributary, the respective maximum meltwater fluxes and melt rates are ∼2 m^3 s^{-1} and ∼50 m a^{-1} for the WAP, and ∼0.2 m^3 s^{-1} and ∼5 m a^{-1} for the EAP. For the EAIS (Fig. 3, light green), melt rates are similar to those observed for the EAP. However, most icebergs calved from the EAIS have tabular geometries (surface areas of ∼0.1–2 km^2) with much larger submerged areas and depths of up to ∼400 m, resulting in larger meltwater fluxes (∼0.5 m^3 s^{-1}) for the peak iceberg melt rates of ∼5 m a^{-1}. Icebergs calved from WAIS are also commonly tabular (surface areas of ∼0.1–3 km^2), but reach depths of up to nearly 800 m and melt rates of ∼40 m a^{-1} (Fig. 3, light pink). As a result of both their high melt rates and large size, the peak iceberg meltwater flux near Thwaites Glacier can exceed 5 m^3 s^{-1}.

Time series of iceberg melt rates with fairly consistent temporal resolution and more than two observation periods are available for 11 of the 15 study sites (Fig. 2 horizontal error bars, Table 1), enabling analysis of temporal variations in iceberg melt rates. Melt rates generally vary with draft and draft distributions vary between observation periods, complicating melt rate
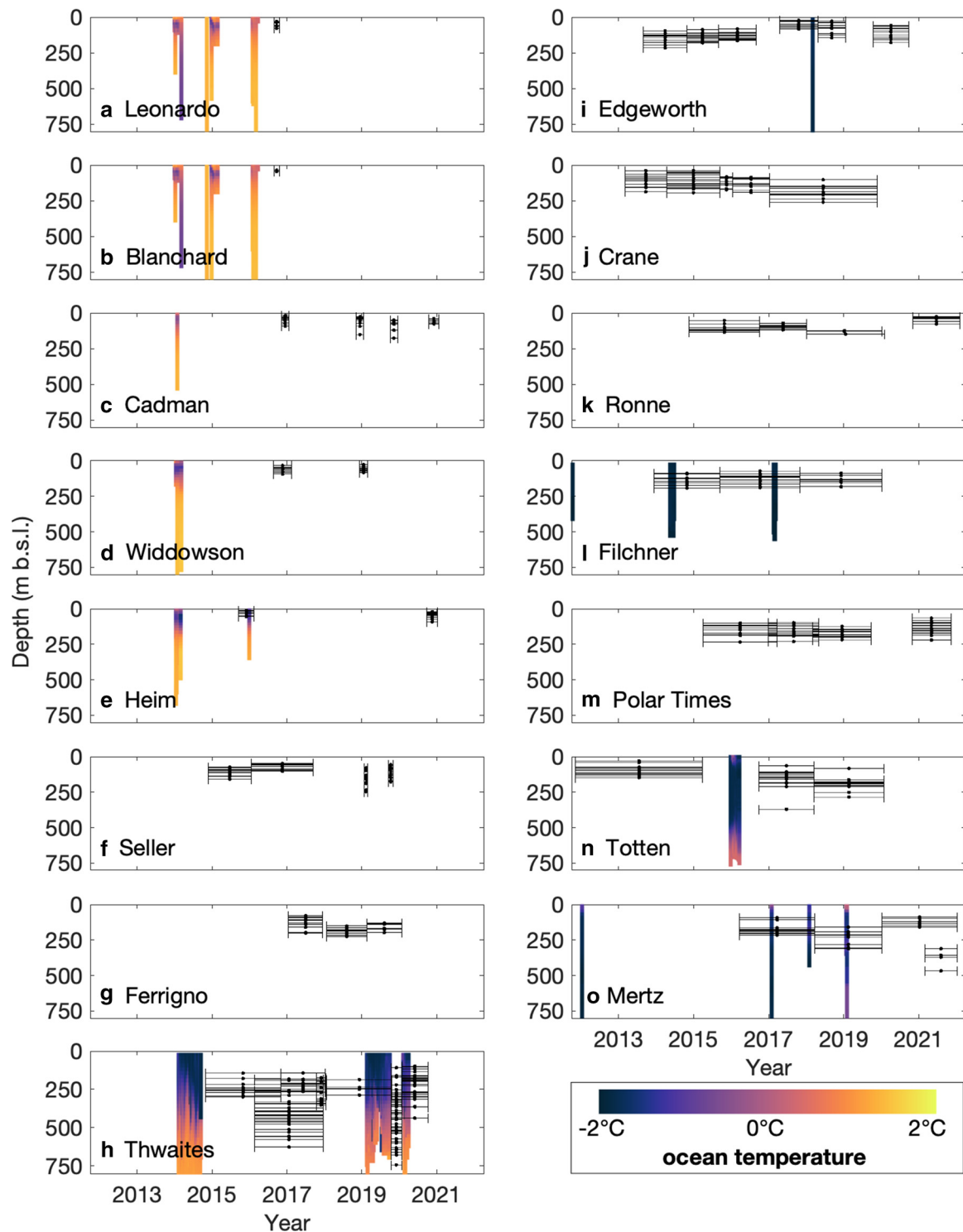
Figure 2. Ocean temperature profile and iceberg observation time series. Colored vertical lines indicate ocean temperature (see color bar). Black symbols indicate the mean draft (*y*-axis), with brackets spanning the observation period (*x*-axis) for icebergs. Panels are arranged geographically, with sites in West Antarctica in the left column and East Antarctica in the right column.

interpretation. Visual, qualitative analysis of the time series of melt rates plotted against draft (Fig. 4) suggests that melt rates are nearly constant across the study period. Quantitatively, we compare the median change in melt rate with draft between observation periods in an effort to account for the draft dependence of melt rates. While the median is less susceptible to biases introduced by outliers than the mean, or analogously the slope of the best-fit linear trendline fit to the melt rate and draft data, variations in melt rate driven by pronounced differences

in environmental conditions across study sites can still bias data. Specifically, we exclude icebergs along the eastern margins of the Thwaites and Mertz floating ice tongues and icebergs with anomalously high melt rates near the Edgeworth terminus from our analysis. The icebergs along the eastern margins of the Thwaites and Mertz ice tongues are fewer in number and farther afield from the termini than the western margin, motivating their removal. The Edgeworth icebergs with anomalously high melt rates are the deepest-drafted icebergs for the study site

Table 2. Summary of ocean observations within 100 km of icebergs

Site name	Profile Count	Unique Date Count	Temperature (°C)			Thermal forcing (°C)		
			Median	Minimum	Maximum	Median	Minimum	Maximum
Edgeworth	3	3	−1.7	−1.7	−1.7	0.2	0.2	0.2
Filchner	909	255	−1.8	−1.9	−1.8	0.1	0.1	0.1
Totten	16	16	−1.5	−1.7	−1	0.5	0.3	0.8
Mertz	322	77	−1.3	−1.8	−0.8	0.7	0.2	1.1
Thwaites	3072	432	−1.5	−1.7	−0.6	0.5	0.2	1.6
Heim	13	7	−1.1	−1.1	−0.8	0.8	0.7	1.1
Widdowson	15	5	−0.4	−0.5	0.3	1.4	1.4	2.1
Cadman	2	1	−0.1	−0.2	0.4	1.8	1.7	2.2
Blanchard	4270	126	−0.3	−0.4	−0.3	1.5	1.5	1.5
Leonardo	2947	122	−0.2	−0.3	−0.2	1.6	1.6	1.7

For each study site with nearby ocean observations (column 1), the number of CTD, APB and ARGO observations (column 2) and number of unique observation dates (column 3) are provided along with metrics to characterize the temperature and thermal forcing (i.e. temperature above the freezing point of water) for all observations (columns 4 and 5, respectively). Temperature and thermal forcing values are averaged over the iceberg depth, then averaged over time, such that the range of values is due to differences in iceberg depth, iceberg observation period and the timing of ocean data acquisitions with respect to iceberg observations.

and are located nearly adjacent to the glacier margin, such that their high melt rates are suggestive of subglacial meltwater plumes and are not representative of melt conditions for the majority of the site's icebergs.

We find that the median increase in melt rate with draft varies regionally such as suggested in Figure 3b – the study site median varies from 0.006 to 0.009 m a^{-1} per m draft for EAP, 0.012–0.021 m a^{-1} per m draft for EAIS, 0.036–0.042 m a^{-1} per m draft for WAIS and 0.10–0.30 m a^{-1} per m draft for WAP – with little temporal variability. There are only two study sites with temporal variations that fall outside of the site-specific median ± the median absolute deviation (i.e. MAD) and cannot be explained by variations in iceberg draft between observation periods: Edgeworth and Ronne. At Edgeworth Glacier, the median increase in melt rate with draft doubled from 2015-16 and 2018-19 (∼0.016 m a^{-1} melt rate per m draft) relative to the 2013–14, 2014–15 and 2019–20 rate (∼0.008 m a^{-1} melt rate per m draft). Along the western margin of the Ronne Ice Shelf, the increase in melt rate with draft was anomalously high

(∼0.03 m a^{-1} melt rate per m draft) in 2017 relative to the median (0.02±0.007 m a^{-1} melt rate per m draft).

Ocean temperatures

While there is still some debate regarding the best parameterization of iceberg melting (FitzMaurice and others, 2016, 2017; Hester and others, 2021), all existing parameterizations model iceberg melt as a function of water temperature. More specifically, the melt rate is assumed to vary with thermal forcing, defined as the temperature of the water relative to its freezing point (Eqn (1)). Ocean temperatures vary considerably between study sites (Fig. 2; Table 2). Temperature profiles from the Weddell Sea (i.e. Edgeworth and Filchner sites) are uniformly cold, such that depth-averaged temperatures are within 0.3°C of the freezing point (i.e. thermal forcing ⩽0.3°C, temperature = [−1.9°C, −1.6°C]) for all icebergs. For Totten and Mertz, seasonal warming is evident in the upper ∼50 m of the water column (Figs 2n, o), resulting in slightly higher depth-averaged temperatures (thermal
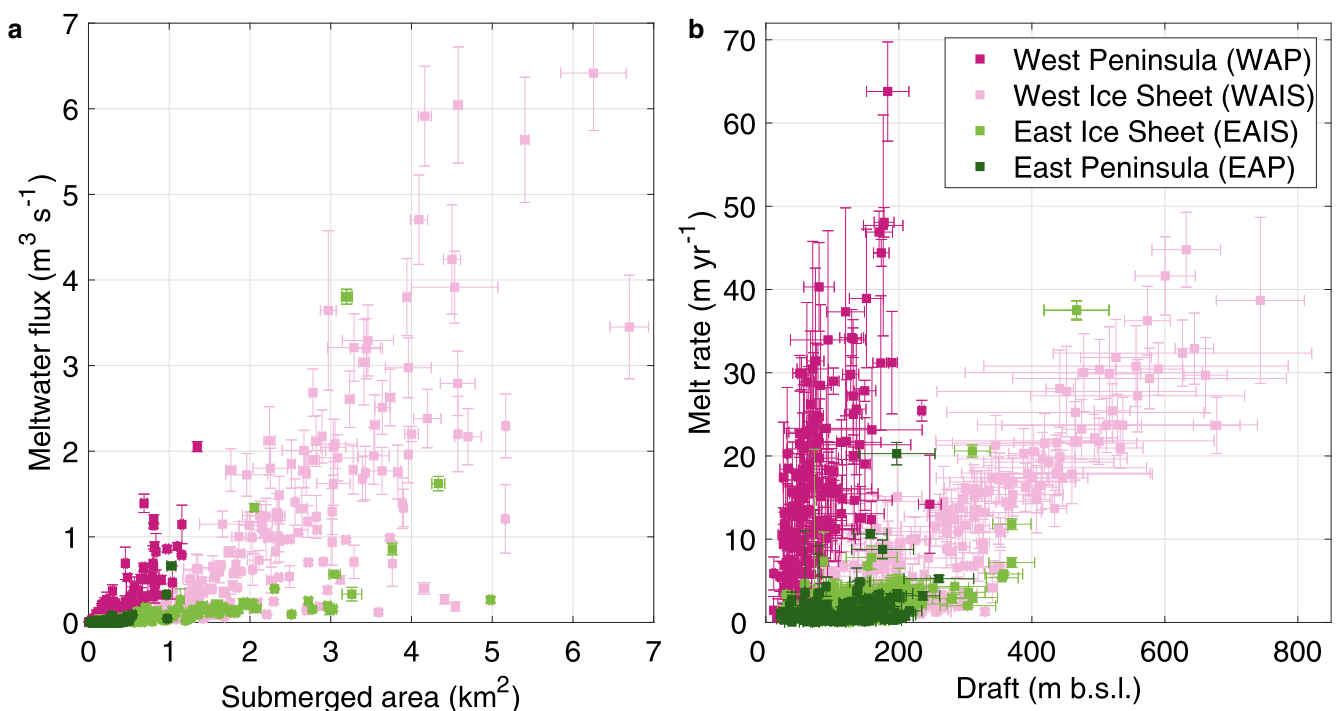

Figure 3. Regional variations in relationships between (a) iceberg meltwater flux and submerged area and (b) iceberg melt rate and draft. Horizontal error bars reflect temporal variations in geometry across the two observation dates and vertical error bars reflect uncertainties in surface elevation change, conversion to volume change, isolation of the submarine melt component and submerged geometry. The same geography-based colormap is used in Figure 1.
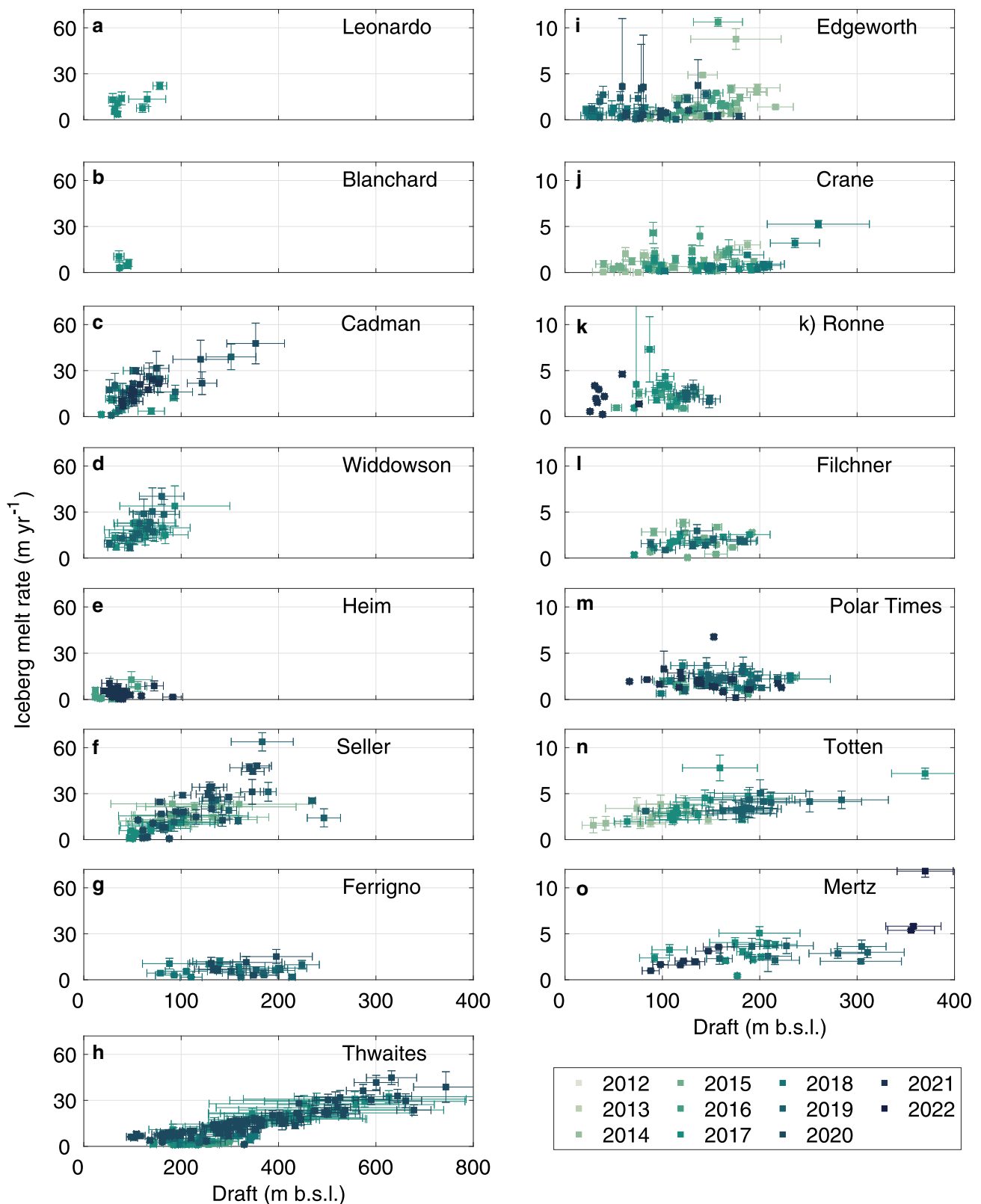
Figure 4. Iceberg melt rate plotted against draft (i.e. depth below sea level). Different *y*-axes scales are used for the (a–h) West Antarctic, (i, j) East Antarctic Peninsula and (k–o) East Antarctic Ice Sheet study sites, excluding outliers for East Antarctica. Horizontal error bars reflect the draft range across the two observation dates and vertical error bars reflect uncertainties in surface elevation change, conversion to volume change, isolation of the submarine melt component and submerged geometry. Symbol colors indicate the central observation year (see legend).

forcing of ~0.6°C). Warmer water is observed at depths >~500 m at Totten, but the icebergs calved from the ice shelf do not reach these depths. At Thwaites, however, the warm subsurface layer can reach depths of ~200 m, such that the majority of the icebergs included in this study penetrate through the colder (<0°C) near-surface layer (Fig. 2h). The ~600 m range in iceberg drafts for Thwaites results in the largest variability in depth-averaged temperatures observed in this study: thermal forcing ranges from 0.2°C for the shallowest icebergs to 1.6°C for icebergs with the deepest drafts. The highest temperatures are generally observed
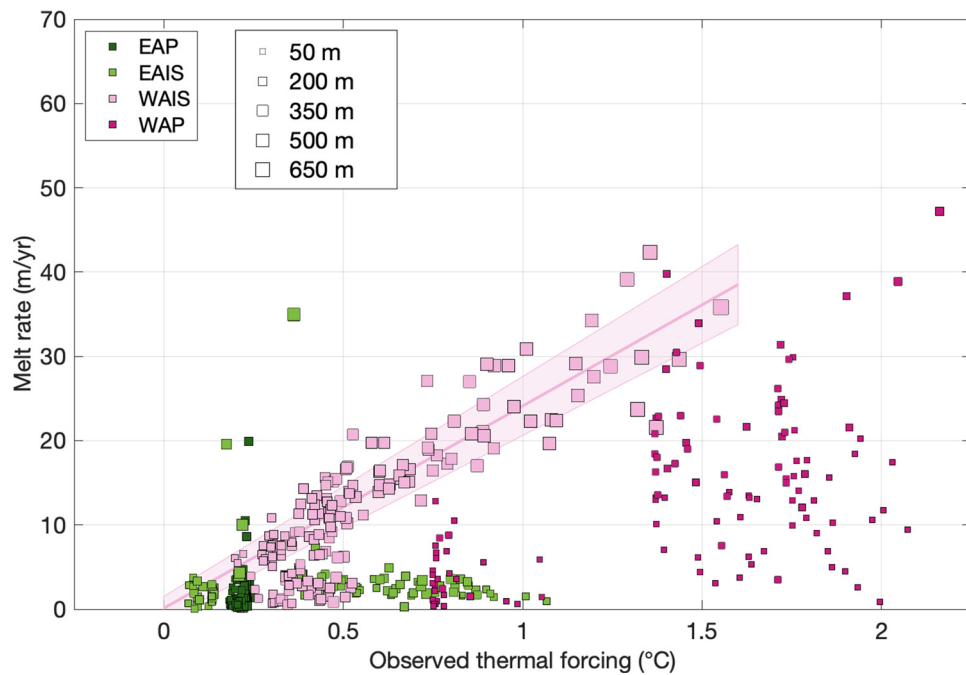
Figure 5. Remotely sensed iceberg melt rates plotted against depth-averaged in situ water temperatures relative to the freezing temperature of the ocean water (i.e. thermal forcing). Symbol sizes vary with draft and colors vary according to region (see legend). The pink line indicates the best-fit linear relationship with 95% confidence intervals (shaded pink region) between melt rate and in situ thermal forcing for Thwaites Glacier.

along the WAP, with temperatures of ∼1°C found within ∼50 m of the surface during austral summer and ∼2°C at depth (below ∼200 m) throughout the year (Figs 2a–e). However, the majority of the icebergs in the region do not penetrate into the warm sub-surface waters – only four of the 115 icebergs from this region have drafts >100 m – such that depth-averaged thermal forcing estimates rarely exceed 2°C.

We find a strong positive linear relationship between iceberg melt rate and observed ocean thermal forcing for Thwaites Glacier (Fig. 5, light pink). For icebergs calved from the western margin of Thwaites, every 1°C increase in thermal forcing equates to an increase in iceberg melt rate of 24 m a^{-1} (R^2 = 0.80, RMSE = 3.7 m a^{-1}°C^{-1}). Thwaites has the largest range in iceberg draft and the most temporally comprehensive ocean temperature record, facilitating the comparison between these independent datasets. Many of the iceberg melt rates for Eastern Antarctica are reasonably approximated by the fit to the Thwaites dataset applied to the observed thermal forcing data (Fig. 5, light green squares), although there are several melt rates that are far higher than expected for the EAIS sites and melt rates that are lower than expected for WAIS and EAIS sites based on thermal forcing relationship observed for Thwaites. Many of the largest icebergs along the WAP adhere to the thermal forcing relationship observed at Thwaites, but there is no apparent relationship between iceberg melt rates and thermal forcing for WAP icebergs with drafts <100 m (Fig. 5, dark pink squares), which might result from the expected higher temporal and spatial variability in upper-ocean temperatures.

Discussion

At the broadest spatial scales, iceberg melt rates vary with ocean temperatures. Estimated melt rates are generally larger along the WAIS/WAP, where ocean waters tend to be warmer, while the smallest melt rates are found in EAIS/EAP. The highest melt rates, observed in the relatively warm waters along the WAP, are far less than melt rates estimated for large icebergs in the open Southern Ocean (Tournadre and others, 2012; Bouhier and others, 2018) but are comparable to the lowest melt rates

observed for Greenland (in the NE). Water temperatures in NE Greenland vary from an approximate minimum of −2°C in the near surface and a maximum of only 1°C located at >200 m depth (Straneo and others, 2012). Along the WAP, we observe similar shelf temperatures, supporting the first-order control of temperature on iceberg melt rates (Fig. 2). The general increase in iceberg melt rates with draft and presence of warm subsurface water masses that can explain the draft dependence of melt rates, as observed around Greenland (Enderlin and others, 2018; Moon and others, 2018), further suggest that iceberg melt rates vary with ocean thermal forcing.

Despite the general agreement between large-scale variations in ocean temperature and iceberg melt rates, we find that thermal forcing alone cannot be used to reliably predict iceberg melt rates around Antarctica. A comparison of melt rates and thermal forcing estimates suggests that a portion of iceberg melt rate variability at Thwaites Glacier can be explained by time- and depth-dependent variations in thermal forcing (Fig. 5, pink shading), yet not all variations in melt rate can be explained as a function of thermal forcing (Fig. 5). The relationship between iceberg melt rate and observation-based thermal forcing estimates varies widely within and across study sites, from near-zero (i.e. melt rates independent of thermal forcing) to ∼100 m a^{-1} increase in iceberg melting per °C increase in thermal forcing. A comparison between iceberg melt rates and modeled thermal forcing estimates (Fig. S2) generally supports the observation-based variability in thermal forcing sensitivity, but with more scatter due to inaccurate thermal forcing estimates. While modeled thermal forcing estimates account for temporal variations in ocean temperature over the full iceberg observation period, the model is constrained by the same sparse ocean temperature data and suffers from coarse spatial resolution and poor knowledge of coastal bathymetry, potentially biasing model outputs. Below we explain how both data uncertainty and errors and variations in the controls on iceberg decay might contribute to the apparent variability in iceberg melt rate sensitivity to thermal forcing.

Uncertainties and/or errors in iceberg melt rates, iceberg draft and time-averaged ocean temperatures all influence the

interpretation of iceberg melt rates in relation to thermal forcing. As described in Dryak and Enderlin (2020), uncertainties in firn density and submerged iceberg area strongly influence the accuracy of iceberg melt rate estimates. Quoted uncertainties in firn density are propagated through the elevation change, meltwater flux and melt rate estimates. However, firn density estimates may be biased, resulting in an unquantifiable but fairly systematic over- or under-estimation of iceberg thicknesses and melt rates for a study site. The assumption of a simple vertical-walled submerged geometry will result in an under-estimation of submerged ice area and over-estimation of iceberg melt rates, but likely by a highly variable amount between icebergs. Quoted uncertainties in firn density are the primary source of uncertainty in melt rates and errors in submerged area likely contribute to the scatter in melt rates for each observation period in Figures 3–4. The iceberg draft error bars in Figures 3–4 do not reflect uncertainties in firn density or submerged area, however, but instead show the range in the best estimate of median iceberg draft across the two observation periods. Thermal forcing is estimated using depth-averaged temperatures over the time-averaged draft and does not account for the change in iceberg draft over time. Estimates of thermal forcing based on the sparse in situ data available in coastal Antarctica also do not fully account for temporal variations in ocean temperature. Because we expect the upper layer temperature of the ocean (100–150 m) to vary more in space and time during the lifespan of an iceberg, sites like the WAP where icebergs were estimated to be relatively shallow while showing a larger range of temperature ranges in the vertical might be particularly susceptible to this source of uncertainty. When all these sources of uncertainty are considered, it is not surprising that there is no consistent relationship between iceberg melt rates and ocean thermal forcing despite the general agreement with large-scale variations in ocean temperature.

Iceberg decay is controlled by physical fragmentation of the iceberg, wave action, surface melting and submarine melt (Bigg and others, 1997; Moon and others, 2018). We exclude icebergs
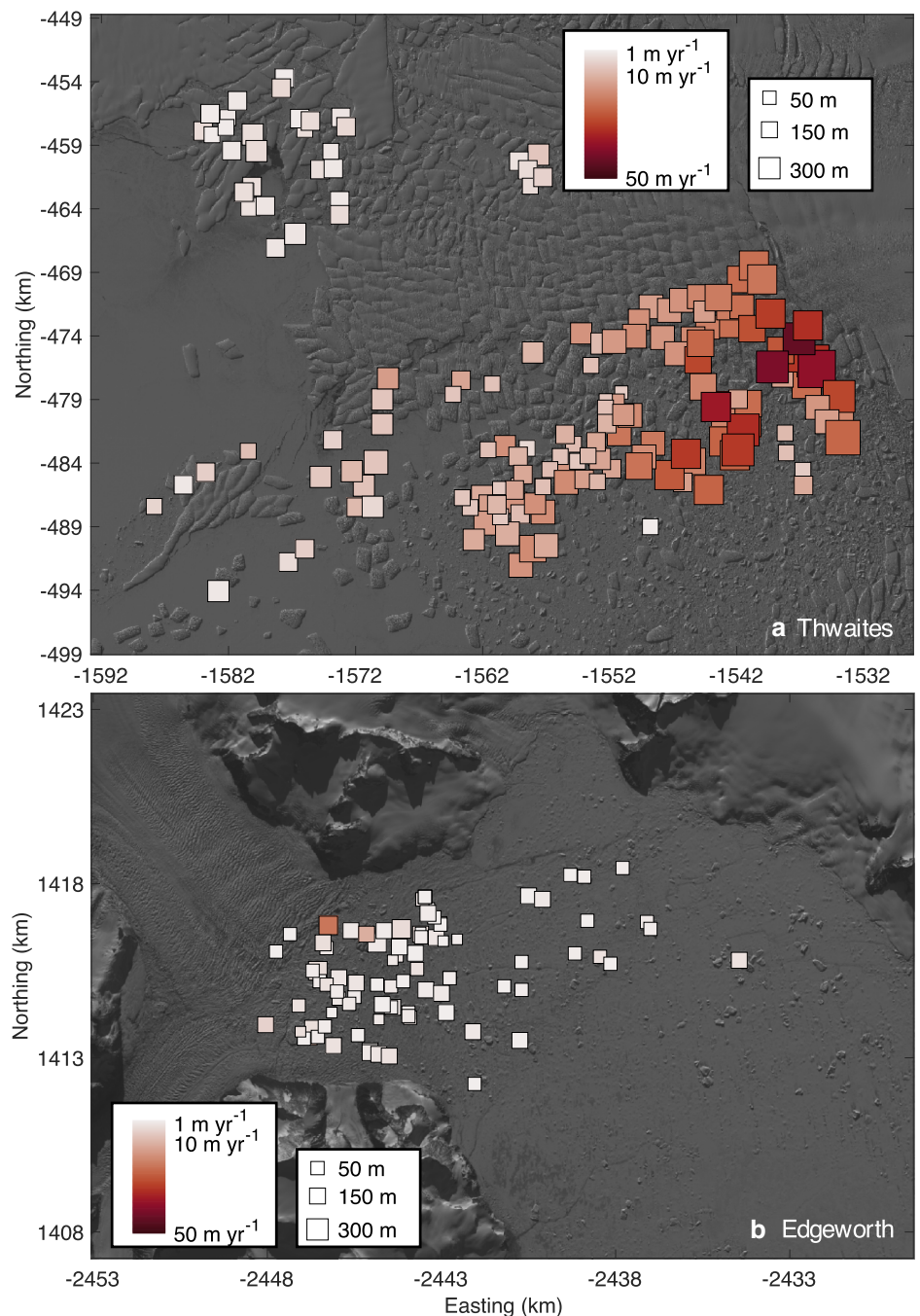

Figure 6. Maps of iceberg melt rate for (a) Thwaites Glacier and (b) Edgeworth Glacier. Symbol color indicates melt rate, where more saturated red corresponds to a faster melt rate, and symbol size indicates median iceberg draft (see legends).

with obvious changes in geometry from our melt estimate process, minimizing the influence of fragmentation on iceberg mass change estimates. Mass loss due to surface meltwater runoff is estimated using surface mass-balance data from the nearest glacierized pixel in the RACMO Antarctica model outputs. We inherently assume that wave action has a negligible influence on mass. While this assumption is valid for the icebergs embedded in mélange or near-persistent sea ice at the EAP, EAIS and WAIS study sites, wave action may strongly influence the mass of the small icebergs transiting the WAP fjords. Finally, even if decay is dominated by submarine melting, the submarine melt rate of an iceberg is dictated by both the relative temperature and velocity of water with respect to the iceberg (Eqn (1)).

Here we assume that thermal forcing is the primary control on iceberg melt rates given the agreement between large-scale variations in iceberg melt rate and temperature observed in Greenland (Enderlin and others, 2018) and in this study, but our results suggest that assumption is overly simplistic. Iceberg melt is driven by both ambient temperature-driven melting as well as shear-driven melting (FitzMaurice and others, 2017; Hester and others, 2021). Both the water temperature and relative velocity vary tremendously in time and space with variations in large-scale ocean properties as well as local modification of water masses. When and where surface meltwater runoff or subglacial melting fluxes are non-negligible, subglacial discharge plumes may considerably alter local water mass properties relative to the regional observations used herein. Submarine melting of both floating ice shelves and tongues (e.g. Drews, 2015; Alley and others, 2016; Gourmelen and others, 2017; Chartrand and Howat, 2020) and grounded termini (e.g. Rignot and others, 2015; Slater and others, 2018; Sutherland and others, 2019) scales non-linearly with subglacial discharge velocities and the increase in water shear caused by the plume (Cowton and others, 2015; Jackson and others, 2017) undoubtedly enhances iceberg melting. At Thwaites, the subglacial discharge plume emanating from its western margin (Alley and others, 2019; Wåhlin and others, 2021) coincides with a localized peak in iceberg melt rate (Fig. 6a, dark red squares). A portion of the spatial variability in Thwaites' melt rates can be explained by variations in iceberg draft, which also drives the strong relationship between melt rate and thermal forcing at the site (Figs 2h, 5), but spatial variations in melt rate remain after accounting for draft dependency. We attribute the draft-independent decrease in melt rate with distance from Thwaites' western margin in part to the dispersion of a semi-persistent discharge plume. We also attribute the anomalous melt rates for icebergs at the margin of Edgeworth Glacier (Fig. 6b, dark red squares) to the presence of a meltwater plume. Although not visible at the surface, the presence of meltwater plumes along the Edgeworth terminus is supported by both the high melt rates of large icebergs near the terminus ($\sim$10–20 m a^{-1}) during two different observation periods as well as the formation of small embayments in the terminus during austral summer. Further work is necessary to assess the potential for subglacial discharge plume mapping from remotely sensed iceberg melt data, but given that many meltwater plumes do not reach the surface but still appreciably impact water mass properties (e.g. Carroll and others, 2016), the prospect of remotely mapping meltwater plumes is compelling.

Conclusions

Iceberg melt rates in coastal Antarctica generally follow large-scale spatial variations in ocean temperature – melt rates are higher along western Antarctica than eastern Antarctica, with an evident increase in melt rates for deeper icebergs in most locations – yet there is no unique, circumpolar relationship between iceberg melt rate and ocean thermal forcing. Furthermore, along the WAP, where the icebergs tend to be shallow, the relationship between

thermal forcing and melt rate is not well defined. Iceberg melt parameterizations that rely on temperature alone are, therefore, unlikely to accurately estimate melt rates. Data limitations may influence the comparison of the iceberg melt rate and independent thermal forcing datasets, but the varying importance of shear-driven iceberg melt likely also contributes to a wide range in melt rates for a given thermal forcing. The importance of shear on melt estimates is most apparent at Edgeworth and Thwaites glaciers, where we attribute localized peaks in iceberg melt rates near the glacier margins to meltwater plume shear-driven enhancement of iceberg melting. If spatial and temporal variations in iceberg melt rates can be more clearly tied to glacier meltwater plumes, potentially at Arctic study sites that are more easily accessible for validation, it may be possible to use time series of iceberg melting to validate modeled surface runoff estimates and provide spatial and temporal constraints on subglacial melting of ice shelves, ice tongues and grounded marine termini.

Finally, although we cannot confidently identify temporal variations in iceberg melt rates due to methodological limitations (i.e. uncertainties in density, depth integration of the melt signal), our comparison of iceberg melt rates with respect to in situ and modeled thermal forcing suggests that melt rates could increase by up to 100 m a^{-1} per 1°C water temperature increase. Given that iceberg melt rates in coastal Antarctica are predominantly <50 m a^{-1}, far below open ocean estimates of up to $\sim$1.5 m d^{-1} ($\sim$500 m a^{-1}), changes in iceberg melting that will likely accompany oceanic warming may drastically alter the spatial distribution of iceberg meltwater fluxes to the Southern Ocean.

References

Alley KE, Scambos TA, Alley RB and Holschuh N (2019) Troughs developed in ice-stream shear margins precondition ice shelves for ocean-driven breakup. *Science Advances* **5**(10), eaax2215. doi: 10.1126/sciadv.aax2215.

Alley K, Scambos T, Siegfried M and Fricker HA (2016) Impacts of warm water on Antarctic ice shelf stability through basal channel formation. *Nature Geoscience* **9**, 290–293. doi: 10.1038/ngeo2675.

Argo (2000) Argo float data and metadata from Global Data Assembly Centre (Argo GDAC). *SEANOE*. doi: 10.17882/42182.

Bigg GR, Wadley MR, Stevens DP and Johnson JA (1997) Modelling the dynamics and thermodynamics of icebergs. *Cold Regions Science and Technology* **26**(2), 113–135. doi: 10.1016/S0165-232X(97)00012-8.

Bindschadler R and 8 others (2008) The Landsat image mosaic of Antarctica. *Remote Sensing of Environment* **112**(12), 4214–4226. doi: 10.1016/j.rse.2008.07.006.

Bouhier N, Tournadre J, Rémy F and Gourves-Cousin R (2018) Melting and fragmentation laws from the evolution of two large Southern Ocean icebergs estimated from satellite data. *The Cryosphere* **12**, 2267–2285. doi: 10.5194/tc-12-2267-2018.

Carroll D and 11 others (2016) The impact of glacier geometry on meltwater plume structure and submarine melt in Greenland fjords. *Geophysical Research Letters* **43**, 9739–9748. doi: 10.1002/2016GL070170.

Chartrand AM and Howat IM (2020) Basal channel evolution on the Getz Ice Shelf, West Antarctica. *Journal of Geophysical Research: Earth Surface* **125**, e2019JF005293. doi: 10.1029/2019JF005293.

Cook AJ and 5 others (2016) Ocean forcing of glacier retreat in the western Antarctic Peninsula. *Science* **353**(6296), 283–286. doi: 10.1126/science.aae0017.

Cowton T, Slater S, Sole A, Goldber A and Nienow P (2015) Modeling the impact of glacial runoff on fjord circulation and submarine melt rate using a new subgrid-scale parameterization for glacial plumes. *Journal of Geophysical Research Oceans* **120**, 796–812. doi: 10.1002/2014JC010324.

DePoorter MA and 6 others (2013) Calving fluxes and basal melt rates of Antarctic ice shelves. *Nature* **502**, 89–92. doi: 10.1038/nature12567.

Drews R (2015) Evolution of ice-shelf channels in Antarctic ice shelves. *The Cryosphere* **9**, 1169–1181. doi: 10.5194/tc-9-1169-2015.

Dryak MC and Enderlin EM (2020) Analysis of Antarctic Peninsula glacier frontal ablation rates with respect to iceberg melt-inferred variability in ocean conditions. *Journal of Glaciology* **66**(257), 457–470. doi: 10.1017/jog.2020.21.

Enderlin EM and 5 others (2018) Greenland iceberg melt variability from high-resolution satellite observations. *The Cryosphere* **12**(2), 565–575. doi: 10.5194/tc-12-565-2018.

Enderlin E, Dryak M and Aberle R (2023) ellynenderlin/iceberg-melt-code: v0.1.1 (v0.1.1). Zenodo. doi: 10.5281/zenodo.8011424.

Enderlin EM and Hamilton GS (2014) Estimates of iceberg submarine melting from high-resolution digital elevation models: applications to Sermilik Fjord, East Greenland. *Journal of Glaciology* **60**, 1084–1092. doi: 10.3189/2014JoG14J085.

Enderlin EM, Hamilton GS, Straneo F and Sutherland DA (2016) Iceberg meltwater fluxes dominate the freshwater budget in Greenland's iceberg-congested glacial fjords. *Geophysical Research Letters* **43**, 11287–11284. doi: 10.1002/2016GL070718.

England MR, Wagner TJ and Eisenman I (2020) Modeling the breakup of tabular icebergs. *Science Advances* **6**(51), eabd1273. doi: 10.1126/sciadv.abd1273.

FitzMaurice A, Cenedese C and Straneo F (2017) Nonlinear response of iceberg side melting to ocean currents. *Geophysical Research Letters* **44**, 5637–5644. doi: 10.1002/2017GL073585.

FitzMaurice A, Straneo F, Cenedese C and Andres M (2016) Effect of a sheared flow on iceberg motion and melting. *Geophysical Research Letters* **43**, 12520–12527. doi: 10.1002/2016GL071602.

Glasser N and Scambos T (2008) A structural glaciological analysis of the 2002 Larsen B ice-shelf collapse. *Journal of Glaciology* **54**(184), 3–16. doi: 10.3189/002214308784409017.

Gourmelen N and 11 others (2017) Channelized melting drives thinning under a rapidly melting Antarctic ice shelf. *Geophysical Research Letters* **44**, 9796–9804. doi: 10.1002/2017GL074929.

Greenbaum J and 9 others (2015) Ocean access to a cavity beneath Totten Glacier in East Antarctica. *Nature Geoscience* **8**, 294–298. doi: 10.1038/ngeo2388.

Hester EW, McConnochie CD, Cenedese C, Couston L-A and Vasil G (2021) Aspect ratio affects iceberg melting. *Physical Review Fluids* **6**(2), 023802. doi: 10.1103/PhysRevFluids.6.023802.

Heywood KJ, Muench R and Williams G (2012) An overview of the synoptic Antarctic shelf-slope interactions (SASSI) project for the International Polar Year. *Ocean Science* **8**(6), 1117–1122. doi: 10.5194/os-8-1117-2012.

Holland DA, Nicholls KW and Basinski A (2020) The Southern Ocean and its interaction with the Antarctic Ice Sheet. *Science* **367**(6484), 1326–1330. doi: 10.1126/science.aaz5491.

Hopwood MJ and 9 others (2019) Highly variable iron content modulates iceberg-ocean fertilisation and potential carbon export. *Nature Communications* **10**, 5261. doi: 10.1038/s41467-019-13231-0.

Jackson RH and 8 others (2017) Near-glacier surveying of a subglacial discharge plume: implications for plume parameterizations. *Geophysical Research Letters* **44**, 6886–6894. doi: 10.1002/2017GL073602.

Jenkins A and 6 others (2016) Decadal ocean forcing and Antarctic ice sheet response: Lessons from the Amundsen Sea. *Oceanography* **29**(4), 106–117. doi: 10.2307/24862286.

Jeong S, Howat IM and Bassis JN (2016) Accelerated ice shelf rifting and retreat at Pine Island Glacier, West Antarctica. *Geophysical Research Letters* **43**, 11720–11725. doi: 10.1002/2016GL071360.

Jongma JI, Driesschaert E, Fichefet T, Goosse H and Renssen H (2009) The effect of dynamic–thermodynamic icebergs on the Southern Ocean climate in a three-dimensional model. *Ocean Modelling* **26**(1–2), 104–113. doi: 10.1016/j.ocemod.2008.09.007.

Khazendar A and 5 others (2013) Observed thinning of Totten Glacier is linked to coastal polynya variability. *Nature Communications* **4**, 2857. doi: 10.1038/ncomms3857.

Ligtenberg SRM, Helsen MM and van den Broeke MR (2011) An improved semi-empirical model for the densification of Antarctic firn. *The Cryosphere* **5**, 809–819, https://doi.org/10.5194/tc-5-809-2011.

Mazloff M, Heimbach P and Wunsch C (2010) An eddy-permitting Southern Ocean State Estimate. *Journal of Physical Oceanography* **40**, 880–899.

McGrath D and 5 others (2012) Basal crevasses on the Larsen C Ice Shelf, Antarctica: implications for meltwater ponding and hydrofracture. *Geophysical Research Letters* **39**, L16504. doi: 10.1029/2012GL052413.

Merino N and 6 others (2016) Antarctic icebergs melt over the Southern Ocean: climatology and impact on sea ice. *Ocean Modelling* **104**, 99–110. doi: 10.1016/j.ocemod.2016.05.001.

Moffat C and Meredith M (2018) Shelf–ocean exchange and hydrography west of the Antarctic Peninsula: a review. *Philosophical Transactions A* **376**, 20170164. doi: 10.1098/rsta.2017.0164.

Moon T and 5 others (2018) Subsurface iceberg melt key to Greenland fjord freshwater budget. *Nature Geoscience* **11**, 49–54. doi: 10.1038/s41561-017-0018-z.

Pritchard HD and 5 others (2012) Antarctic ice-sheet loss driven by basal melting of ice shelves. *Nature* **484**, 502–505. doi: 10.1038/nature10968.

Rignot E, Fenty I, Xu Y, Cai C and Kemp C (2015) Undercutting of marine-terminating glaciers in West Greenland. *Geophysical Research Letters* **42**, 5909–5917. doi: 10.1002/2015GL064236.

Rignot E, Jacobs S, Mouginot J and Scheuchl B (2013) Ice-shelf melting around Antarctica. *Science* **341**(6143), 266–270. doi: 10.1126/science.1235798.

Sallée J-B (2018) Southern Ocean warming. *Oceanography* **31**(2), 52–62.

Scambos TA and 6 others (2014) Detailed ice loss pattern in the northern Antarctic Peninsula: widespread decline driven by ice front retreats. *The Cryosphere* **8**, 2135–2145. doi: 10.5194/tc-8-2135-2014.

Scambos TA, Bohlander JA, Shuman CA and Skvarca P (2004) Glacier acceleration and thinning after ice shelf collapse in the Larsen B embayment, Antarctica. *Geophysical Research Letters* **31**, L18402. doi: 10.1029/2004GL020670.

Schmidtko S, Heywood KJ, Thompson AF and Aoki S (2014) Multidecadal warming of Antarctic waters. *Science* **346**(6214), 1227–1231. doi: 10.1126/science.1256117.

Schwarz JN and Schodlok MP (2009) Impact of drifting icebergs on surface phytoplankton biomass in the Southern Ocean: ocean colour remote sensing and in situ iceberg tracking. *Deep Sea Research Part I: Oceanographic Research Papers* **56**, 1727–1741. doi: 10.1016/j.dsr.2009.05.003.

Shean DE and 6 others (2016) An automated, open-source pipeline for mass production of digital elevation models (DEMs) from very high-resolution commercial stereo satellite imagery. *ISPRS Journal of Photogrammetry and Remote Sensing* **116**, 101–117. doi: 10.1016/j.isprsjprs.2016.03.012.

Shuman CA, Berthier E and Scambos TA (2011) 2001–2009 elevation and mass losses in the Larsen A and B embayments, Antarctic Peninsula. *Journal of Glaciology* **57**(204), 737–754. doi: 10.3189/002214311797409811.

Slater DA and 5 others (2018) Localized plumes drive front-wide ocean melting of a Greenlandic tidewater glacier. *Geophysical Research Letters* **45**, 12350–12358. doi: 10.1029/2018GL080763.

Smith KL and 7 others (2007) Free-drifting icebergs: hot spots of chemical and biological enrichment in the Weddell Sea. *Science* **317**, 478–482. doi: 10.1126/science.1142834.

Smith KL, Sherman AD, Shaw TJ and Sprintall J (2013) Icebergs as unique Lagrangian ecosystems in polar seas. *Annual Review of Marine Science* **5**, 269–287. doi: 10.1146/annurev-marine-121211-172317.

Straneo F and 8 others (2012) Characteristics of ocean waters reaching Greenland's glaciers. *Annals of Glaciology* **53**(60), 202–210. doi: 10.3189/2012AoG60A059.

Sutherland DA and 8 others (2019) Direct observations of submarine melt and subsurface geometry at a tidewater glacier. *Science* **365**(6451), 369–374. doi: 10.1126/science.aax3528.

Tournadre J, Girard-Ardhuin F and Legrésy B (2012) Antarctic icebergs distributions, 2002–2010. *Journal of Geophysical Research* **117**, C05004. doi: 10.1029/2011JC007441.

Treasure A and 27 others (2017) Marine mammals exploring the oceans pole to pole: a review of the MEOP consortium. *Oceanography* **30**(2), 132–138. doi: 10.5670/oceanog.2017.234.

Wåhlin AK and 8 others (2021) Pathways and modification of warm water flowing beneath Thwaites Ice Shelf, West Antarctica. *Science Advances* **7**, eabd7254. doi: 10.1126/sciadv.abd7254.

Weeks W and Campbell W (1973) Icebergs as a fresh-water source: an appraisal. *Journal of Glaciology* **12**(65), 207–233. doi: 10.3189/S0022143000032044.

Wu S-Y and Hou S (2017) Impact of icebergs on net primary productivity in the Southern Ocean. *The Cryosphere* **11**, 707–722. doi: 10.5194/tc-11-707-2017.